

Superconducting single-electron transistor coupled to a two dimensional electron gas: Transmission lines, dissipation, and charge averaging

A. J. Rimberg^{1,2} and W. Lu¹

¹*Department of Physics and Astronomy, Rice University, Houston, Texas 77005*

²*Department of Electrical and Computer Engineering, Rice University, Houston, Texas 77005*

We have developed a novel system consisting of a superconducting single-electron transistor (S-SET) coupled to a two-dimensional electron gas (2DEG), for which the dissipation can be tuned in the immediate vicinity of the S-SET. To analyze our results, we have developed a model of the environment for S-SET/2DEG systems that includes electromagnetic fluctuations coupled both through the S-SET leads and capacitively to the S-SET central island. We analyze this model, treating the leads as finite transmission lines, to find the probability function $P(E)$ for exchanging energy E with the environment. We also allow for the possibility of low-frequency fluctuations of the S-SET offset charge. We compare our calculations with measurements of SET conductance versus 2DEG conductance and find good agreement for temperatures > 100 mK, while unexplained discrepancies emerge for lower temperatures. By including the effects of charge averaging we are also able to predict the shape and evolution of I - V curves as the 2DEG in the vicinity of the S-SET is changed.

PACS numbers: 74.50.+r, 73.23.Hk, 74.40.+k

I. INTRODUCTION

The effects of the electromagnetic environment on electric transport has been a subject of extensive theoretical and experimental interest in recent years. The reasons for interest are varied, as are the systems for which studies of the effects of the environment have been performed. Recent interest in quantum computation^{1,2,3,4} has prompted interest in the effects of dissipation on decoherence rates in superconducting qubits.^{5,6} Double quantum dots have been used to study the effects of the environment on inelastic tunneling rates,⁷ and have been proposed as detectors of high-frequency noise produced by mesoscopic devices.⁸ Finally, interest in quantum phase transitions⁹ has prompted study of the effects of dissipation on superconducting systems such as thin films^{10,11} and Josephson junction arrays.¹²

Given the possibility of using a single Cooper pair box^{2,13} as a qubit and its similarity to the superconducting single-electron transistor (S-SET),¹⁴ it seems logical to use the S-SET as a model system for studying the effects of environmental dissipation on coherence and transport in small tunnel junction systems. Recently, there have been several such attempts, motivated by experiments in which a Josephson junction array was fabricated in close proximity to a two-dimensional electron gas (2DEG) in an GaAs/Al_xGa_{1-x}As heterostructure,¹² which can be used as a tunable source of dissipation. (While the effects of a mechanically tunable environment were earlier studied in the macroscopic quantum tunneling regime,¹⁵ use of a 2DEG allows more flexible tuning of the environment over a larger impedance range.) In place of an array, we and the Berkeley group have instead used similar fabrication techniques to couple an S-SET to a 2DEG.^{16,17,18} In one instance, the focus was on transport at higher biases, in the regime of the Josephson-quasiparticle cycle.¹⁷ In the others, the focus instead was

on the low bias regime and the tunneling rates of Cooper pairs.^{16,18} Theoretical work aimed at an explanation of the results of the Berkeley group was undertaken by Wilhelm, *et al.*¹⁹

The primary experimental difference between our own work and that of the Berkeley group lies in the way in which the environment is varied. The Berkeley group followed an approach developed earlier for the study of junction arrays,¹² using a gate on the back side of the substrate to vary the sheet density n_s of the 2DEG, and therefore its resistance per square R_{sq} . Such a change is global, and affects the 2DEG not only immediately beneath the S-SET, but beneath the macroscopic leads used to measure it as well. In our own work, by placing Au gates on the surface of the sample near the S-SET itself, we were able to vary the dissipation in the 2DEG locally, while leaving 2DEG beneath the leads virtually unchanged.^{18,20}

The Berkeley group compared their results to the theory of Wilhelm, *et al.*, which predicted that within linear response the conductance G_{SET} of the S-SET would scale with the ground plane conductance $G_{2D} = 1/R_{sq}$ and temperature T as G_{2D}^β/T^α . While the Berkeley group did observe power law behavior, their measured exponents were not in quantitative agreement with theory. Furthermore, the measured β depended on T and α on G_{2D} , calling the scaling form into question.

In our own work,¹⁸ we examined a somewhat more complex model for the environment than that considered by Wilhelm, *et al.* Specifically, we allowed for coupling of electromagnetic fluctuations to tunneling Cooper pairs due simultaneously both to the S-SET leads and to the 2DEG in the immediate vicinity of the S-SET, which is coupled to the S-SET central island via a capacitance C_{2D} . By also allowing for averaging of the S-SET offset charge, we were able to obtain good agreement between our measurements and calculations. Here we examine

our model of the environment in somewhat more detail, provide additional experimental data which supports our earlier analysis, and also give some additional details of the calculation.

II. SAMPLE AND ENVIRONMENTAL CALCULATIONS

A. Sample Design and the Environmental Model

1. Sample Design

Our samples consist of an Al/AIO_x-based S-SET fabricated in close proximity to a 2DEG formed in a GaAs/Al_xGa_{1-x}As heterostructure²⁰ as shown in Fig. 1 below. We begin by fabricating six Au gates which can be used to deplete the electrons beneath them by application of a negative gate voltage V_g . At the center of the Au gates we then fabricate our S-SET, as can be seen in the electron micrograph (expanded view in Fig. 1). Note that as shown in the larger diagram the S-SET leads extend over the 2DEG to macroscopic contact pads. For the vast majority of their length they are well away from the Au gates and the 2DEG beneath them is independent of V_g . When we apply a gate voltage V_g to all six Au gates, the electrons immediately beneath them are depleted, leaving a small pool of electrons beneath the S-SET. This pool is connected to the rest of the 2DEG (held at ground) only by two quantum point contacts (QPCs) with conductances $1/R_{\text{QPC}}$ (assumed equal) as shown in the micrograph. It is also capacitively coupled to the S-SET island through a capacitance C_{2D} as shown in the lower right inset to Fig. 1. When all six Au gates are energized as described above, we say that the electrons are confined in the “pool” geometry. We do not refer to the pool as a quantum dot since for these experiments the QPCs are sufficiently open that no Coulomb oscillations are detected in the pool and discrete energy levels have not formed.

Because the Au gates can be biased independently, we can also apply V_g to only the four outermost gates which form the QPCs. As before, the electrons beneath the S-SET are coupled to ground through the QPCs. In addition, however, they are now coupled through a resistance R_{str} to two large reservoirs of electrons located between the four outermost gates, as can be seen in Fig. 1. The reservoirs are in turn coupled to ground only through a capacitance C_{str} . When only the four outer gates are energized, we say that the electrons in the 2DEG are confined in the “stripe” geometry. We observe significant differences between the measured S-SET conductance G_{SET} versus applied gate voltage V_g for the two different geometries, as will be discussed below.

Regardless of the gate configuration used, we can apply a single model of the environment to our results, as shown in the lower left in Fig. 1. The SET island is connected to its leads through junctions with resistance

$R_{1(2)}$ and capacitance $C_{1(2)}$. We assume that the S-SET leads present an impedance Z_ℓ to the SET while the 2DEG electrons have a total impedance Z_{2D} to ground which is coupled to the SET through the capacitance C_{2D} . Nearly the entire length of the SET leads is far from the Au gates, so that Z_ℓ is almost completely unaffected by the gate voltage V_g . The electrons immediately beneath the SET are strongly affected by V_g so that Z_{2D} will in general be a function of V_g , and may also depend on the configuration of gates used (*i. e.*, on the pool versus stripe geometry). Finally, the SET is also coupled to the Au gates by a capacitance C_g . We neglect the possibility of a substantial impedance on the gate lines largely because $C_g \approx 20$ aF is by far the smallest capacitance in the problem. Furthermore, any gate impedance would be substantially reduced since there are six gates whose impedances would combine in parallel. This general model (excluding the small gate capacitance C_g) has been investigated previously,^{21,22} but without considering any particular form for the impedances Z_ℓ and Z_{2D} .

In Table I below we give the relevant sample parameters for the two samples S1 and S2 considered here. The parameters were determined from electrical measurement and simulations as discussed elsewhere.¹⁷

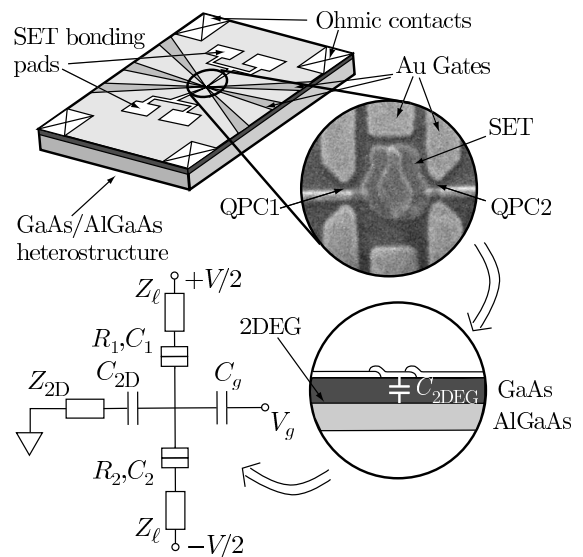


FIG. 1: Schematic diagram of a typical sample, showing the Au gates, Ohmic 2DEG contacts, and SET leads and bonding pads. The upper right inset is an electron micrograph showing the S-SET island surrounded by the six Au gates. Application of a gate voltage V_g causes QPCs to form at the locations shown. The S-SET is coupled to the 2DEG beneath it by a capacitance C_{2D} as illustrated in the lower right inset. In the lower left we show a circuit diagram of our model of the S-SET environment, including the lead impedances Z_ℓ and the impedance Z_{2D} associated with the electrons immediately beneath the S-SET, coupled to it through the capacitance C_{2D} . We also show the combined capacitance C_g to the six Au gates.

TABLE I: Parameters for samples S1 and S2. Capacitances are in aF and energies in μeV .

sample	C_1	C_2	C_g	C_{2D}	E_c	E_{J_1}	E_{J_2}
S1	181	120	20	356	118	5.9	3.5
S2	375	260	20	382	77	27.	16.

2. Tunneling Rates

In general for our samples the charging energy $E_c = e^2/2C_\Sigma$ where $C_\Sigma = C_1 + C_2 + C_g + C_{2D}$ satisfies $E_{J_j} < E_c \ll k_B T$, where $E_{J_j} = \frac{R_Q}{2R_j} \Delta$ is the Josephson energy of junction j given by the Ambegaokar-Baratoff relation²³ and Δ is the superconducting gap. Under these circumstances the S-SET island charge is well defined, so that charge states can be used as the basis for calculating the tunneling rates.^{24,25} We will also be concerned with transport at sufficiently low bias voltages V and temperatures T , that we need only consider the tunneling of Cooper pairs, for which the sequential tunneling rate through junction j is given by²⁶

$$\Gamma(\delta f^{(j)}) = (\pi/2\hbar) E_{J_j}^2 P(-\delta f^{(j)}) \quad (1)$$

which is valid for $E_{J_j} \ll E_c$. Here $\delta f^{(j)} = f_f - f_i$ is the change in free energy associated with the tunneling event, and the function $P(E)$ describes the probability of the Cooper pair exchanging an energy E with the electromagnetic environment during the tunneling process. Following the usual environmental theory,²⁴ $P(E)$ can be expressed in terms of the real part of the total impedance seen by the tunneling electron $\text{Re}[Z_t(\omega)]$ first through a

kernel $K(t)$

$$K(t) = R_Q^{-1} \int_{-\infty}^{\infty} \frac{d\omega}{\omega} \text{Re}[Z_t(\omega)] \times \left\{ \coth\left(\frac{\hbar\omega}{2k_B T}\right) [\cos(\omega t) - 1] - i \sin(\omega t) \right\} \quad (2)$$

and then through the Fourier transform

$$P(E) = \frac{1}{2\pi\hbar} \int_{-\infty}^{\infty} dt \exp[K(t) + iEt/\hbar]. \quad (3)$$

A calculation of the tunneling rate Γ must therefore begin with a clear understanding of the impedance $Z_t(\omega)$ presented to the tunneling electrons by the environment.

3. Model of the Environment

Given the circuit model shown in Fig. 1, one can use standard network analysis²⁷ to calculate the impedance $Z_t(\omega)$ seen by an electron tunneling through junction j in terms of the impedances and capacitances shown in Fig. 1. The result is given by²¹

$$Z_t(\omega) = \frac{1}{i\omega\tilde{C} + \tilde{Y}} \quad (4)$$

where

$$\tilde{C} = \frac{C_\Sigma C_j}{C_{j'} + C_{2D}} \quad (5)$$

where $j' = 2(1)$ for $j = 1(2)$ and

$$\tilde{Y} = \frac{C_\Sigma^2}{(C_{j'} + C_{2D})C_{j'}C_{2D}} \frac{(C_{j'} + C_{2D})C_{j'}C_{2D} + i\omega(C_{j'}C_{2D})^2(Z_\ell + Z_{2D})}{[(C_{j'} + C_{2D})^2 + C_{j'}^2]Z_\ell + C_{2D}^2Z_{2D} + i\omega(C_{j'} + C_{2D})C_{j'}C_{2D}(Z_\ell + 2Z_{2D})Z_\ell} \quad (6)$$

ignoring terms of order C_g/C_{2D} . To proceed, we need accurate models of Z_ℓ and Z_{2D} ; we begin by considering Z_ℓ .

4. Model of Z_ℓ

Since our leads are fabricated above the 2DEG, which acts as a ground plane, it is appropriate to model them as transmission lines.²⁸ The most general form for the impedance Z_{tr} of a lossy transmission line terminated in a load Z_L is given by

$$Z_{\text{tr}} = Z_0 \frac{Z_L + Z_0 \tanh \gamma \ell}{Z_0 + Z_L \tanh \gamma \ell} \quad (7)$$

where Z_0 is the characteristic impedance of the line, γ its complex propagation constant and ℓ its length. At the relatively low frequencies ($\lesssim 10^{11}$ Hz) considered here, it is reasonable to ignore the inductive reactance of the line and treat it as a simple RC line with a resistance and capacitance per unit length r_ℓ and c_ℓ . Doing so, we have that $Z_0 = \sqrt{r_\ell/i\omega c_\ell}$ and $\gamma = \sqrt{i\omega c_\ell r_\ell}$. Looking out at the line from the sample, the line termination Z_L is provided by the bias circuitry, which typically presents a low impedance $\lesssim 50 \Omega$. For simplicity we therefore take $Z_L = 0$ in Eq. (7), and obtain the resulting approximation

$$Z_{RC}(\omega) = \sqrt{\frac{r_\ell}{i\omega c_\ell}} \tanh \sqrt{i\omega r_\ell c_\ell} \ell^2 \quad (8)$$

which we take as the basic form for the impedance of a finite RC line. This form has been considered previously in the context of incoherent tunneling of Cooper pairs in individual Josephson junctions.²⁹

While this is likely a fairly accurate description of the impedance of a section of our leads, when used in evaluating the kernel $K(t)$ in (2) it leads to integrals which are analytically intractable. Fortunately a further simplification is possible. We are interested in the low energy part of $P(E)$, which we expect from (3) to be dominated by the long time behavior of $K(t)$, which is in turn dominated by the low frequency part of the impedance Z_{RC} . We therefore expand Eq. (8) around $\omega = 0$ to obtain

$$Z_{RC}(\omega) \approx \frac{r_\ell \ell}{1 + (\omega r_\ell c_\ell \ell^2 / \sqrt{6})^2} \quad (9)$$

as a reasonable approximation to Z_{RC} in the interesting limit.

Another common treatment²⁵ of the RC transmission line problem is to consider an infinite RC line, whose impedance is given by $Z_0 = \sqrt{r_\ell / i\omega c_\ell}$. Unlike the finite RC line, for which the impedance Z_{RC} approaches a constant $r_\ell \ell$ at $\omega = 0$, the infinite RC line has a $1/\sqrt{\omega}$ singularity at $\omega = 0$ which dominates the long-time limit of $K(t)$ and therefore $P(E)$. The kernel $K(t)$ for the infinite line, as well as $P(E)$, can be calculated exactly in the $T = 0$ limit. At non-zero temperatures, a high-temperature expansion must be performed instead.¹⁹

5. Model of Z_{2D}

Having developed a model for Z_ℓ , we now consider a model for Z_{2D} . The particular model will depend on the geometry we choose. For an unconfined 2DEG, the simplest choice is that Z_{2D} is ohmic with an impedance related to R_{sq} of the 2DEG: $Z_{2D} \approx R_{sq}/3$. When the electrons are confined in the pool geometry, they are coupled to the remaining 2DEG by two QPCs with conductance $1/R_{QPC}$ (assumed equal), which appear in parallel from the vantage point of the SET. There is likely some shunt capacitance C_{QPC} as well, but the associated roll-off frequency $1/R_{QPC}C_{QPC}$ is typically large ($\sim 10^{11}$ s⁻¹) and we therefore neglect it. So for the pool geometry, we take

$$Z_{2D} = R_{QPC}/2. \quad (10)$$

The stripe geometry is more complex. Here, in addition to the QPC conductances, the electrons beneath the SET are coupled to two large electron reservoirs with resistance R_{str} located between the outermost Au gates. At their narrowest, the reservoirs are $0.6 \mu\text{m}$ wide, but broaden in five sections to a width of $500 \mu\text{m}$. Each section contributes roughly $2R_{sq}$, so that $R_{str} \approx 10R_{sq} = 200 \Omega$. These reservoirs are in turn coupled to ground capacitively through a capacitance C_{str} , which we estimate from the size of the reservoirs to be on the order of 0.3 pF. Using $Z_{2D}^{-1} = 2(R_{QPC}^{-1} + Z_{str}^{-1})^{-1}$ where

$Z_{str} = R_{str} + 1/i\omega C_{str}$ we find

$$\text{Re}[Z_{2D}] = \frac{R_{QPC}}{2} \left[\frac{1 + \omega^2 \tau_{str}^2 R_{str} / (R_{QPC} + R_{str})}{1 + \omega^2 \tau_{str}^2} \right] \quad (11)$$

where $\tau_{str} = C_{str}(R_{str} + R_{QPC})$. For $\omega^2 \tau_{str}^2 \ll 1$, then, $\text{Re}[Z_{2D}]$ approaches $R_{QPC}/2$, while for $\omega^2 \tau_{str}^2 \gg 1$, $\text{Re}[Z_{2D}]$ approaches $\frac{1}{2}(R_{str}^{-1} + R_{QPC}^{-1})^{-1}$. The imaginary part of Z_{2D} in the stripe geometry is nonnegligible only in the vicinity of $\omega \sim 1/\tau_{str}$, so for our purposes we neglect it. In general then, at low frequencies $\text{Re}[Z_{2D}]$ is kept finite by the presence of the QPCs, and at higher frequencies is dominated by the smaller of $R_{QPC}/2$ and $R_{str}/2$.

6. Decomposition of $Z_t(\omega)$

While the form for $Z_t(\omega)$ given by Eqs. (4)–(6) is complete, it is generally too complex to make significant headway in calculating $K(t)$. Fortunately, significant simplification is possible. For typical values of $r_\ell \approx 1 \times 10^6 - 1 \times 10^7 \Omega/\text{m}$ and typical line lengths $\ell \approx 0.5 - 1$ mm, $Z_\ell \gg Z_{2D}$ for small ω . In contrast, for sufficiently large ω , Z_{RC} becomes quite small ($\lesssim 10 \Omega$) and the condition $Z_{2D} \gg Z_\ell$ is usually satisfied. It then becomes possible to decompose \tilde{Y} in Eq. (6) into a low ω part dominated by Z_ℓ and a high ω part dominated by Z_{2D} .

For small ω , as long as $Z_\ell \gg Z_{2D}$, we can safely neglect the terms in Eq. (6) involving Z_{2D} . Furthermore, for ω such that $\omega \ll \min(1/C_j Z_\ell, 1/C_{2D} Z_\ell)$ we can ignore terms in Eqs. (4) and (6) that depend explicitly on ω . Making these simplifications, we have that in the small ω , large Z_ℓ limit

$$Z_t(\omega) \approx \tilde{Y}^{-1} = \frac{(C_{j'} + C_{2D})^2 + C_{j'}^2}{C_\Sigma} Z_\ell \equiv \kappa_1 Z_\ell. \quad (12)$$

For large ω , we drop terms of order Z_ℓ/Z_{2D} , and find that we can neglect the explicit frequency dependence in the denominator of (6) for $\omega \ll c_\ell/(C_{j'})^2 r_\ell \sim 1 \times 10^{16}$ rad/s. In contrast, we cannot necessarily neglect the explicit frequency dependence in the numerator, and find

$$\tilde{Y} \approx \left(\frac{C_\Sigma}{C_{2D}} \right)^2 \frac{1}{Z_{2D}} + i\omega \frac{C_\Sigma^2 C_{j'}}{(C_{j'} + C_{2D}) C_{2D}}. \quad (13)$$

We combine this with (4) to find in this limit

$$Z_t(\omega) = \frac{1}{i\omega(C_1 + C_2)C_\Sigma/C_{2D} + (C_\Sigma/C_{2D})^2 Z_{2D}^{-1}} \equiv \frac{1}{i\omega C_{\text{eff}} + \kappa_2^{-1} Z_{2D}^{-1}}. \quad (14)$$

Combining this result with (12), we obtain for the real part of $Z_t(\omega)$

$$\text{Re}[Z_t(\omega)] = \kappa_1 \text{Re}[Z_\ell(\omega)] + \frac{\kappa_2 Z_{2D}}{1 + [\omega C_{\text{eff}} \kappa_2 Z_{2D}]^2}, \quad (15)$$

which we take as our basic model for the real part of the impedance seen by an S-SET fabricated above a 2DEG ground plane. We believe this model should be applicable not only to our own system, but to that of the Berkeley group as well.¹⁶

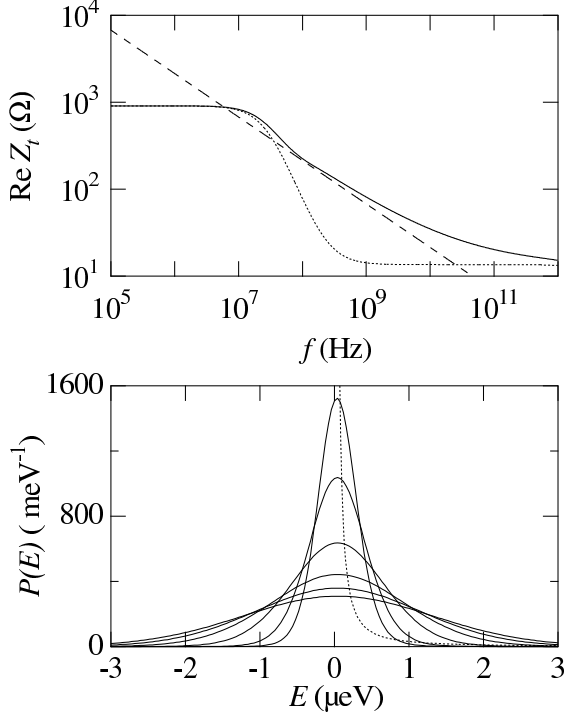


FIG. 2: (a) $\text{Re}[Z_t(\omega)]$ for three different environmental models, all based on a transmission line with $r_\ell = 2.9 \times 10^6 \, \omega/\text{m}$ and $c_\ell = 1.0 \times 10^{-8} \, \text{F/m}$ and $\ell = 6.94 \times 10^{-4} \, \text{m}$. For this graph we have used $Z_{2D} = 100 \, \Omega$. Solid line: exact result based on the full forms for $Z_t(\omega)$ and Z_ℓ . Dotted line: approximate form based on the low frequency approximation to Z_ℓ and the decomposition of $\text{Re}[Z_t(\omega)]$. Dashed line: infinite line result for the same values of r_ℓ and c_ℓ . (b) Solid lines: $P_s(E)$ for the same transmission line parameters, for (top to bottom) $T = 10, 20, 50, 100, 150$, and $200 \, \text{mK}$. Dashed line: $P(E)$ for an infinite RC line at $T = 0$.

To illustrate the degree of approximation associated with Eqs. (9) and (15), we show in Fig. 2(a) $\text{Re}[Z_t(\omega)]$ for three separate models of the environment; all are based on an RC line with $r_\ell = 2.9 \times 10^6 \, \omega/\text{m}$ and $c_\ell = 1 \times 10^{-8} \, \text{F/m}$. The solid line shows $\text{Re}[Z_t(\omega)]$ based on Eqs. (4)–(6) and Eq. (8), *i. e.*, on the impedance of a finite RC line coupled to a ground plane with impedance

Z_{2D} , using the full form for $\text{Re}[Z_t(\omega)]$. The dotted line is $\text{Re}[Z_t(\omega)]$ calculated using the low-frequency version of Z_ℓ given in (9) and using the decomposition (15) of $\text{Re}[Z_t(\omega)]$, while the dashed line is the impedance of an infinite RC line using the same values of r_ℓ and c_ℓ (with no ground plane). We have not included a curve using the decomposition (15) and the exact form for a finite RC line in (8) since it is virtually indistinguishable from the full $\text{Re}[Z_t(\omega)]$ shown.

We note that the impedance of the infinite line rises above that of the more realistic forms for frequencies below a few MHz, so that in general it gives more weight to the low frequency modes and may be expected to give a more sharply peaked $P(E)$. More importantly, the low-frequency approximation to Z_ℓ , while agreeing quite well below $\sim 10^7 \, \text{Hz}$ with the exact finite line result, significantly underestimates it for intermediate frequencies below $\sim 10^{12} \, \text{Hz}$. The approximation may therefore be of limited use for larger bias voltages; for low biases, however, it is likely to be more accurate than a model based on an infinite transmission line, which overestimates the impedance at low frequencies. Finally, at sufficiently high frequencies, the approximate and exact forms for $\text{Re}[Z_t(\omega)]$ converge.

B. Calculation of $K(t)$ and $P(E)$

1. Calculation of $K(t)$

Having produced a tractable form for $\text{Re}[Z_t(\omega)]$, we can now proceed to a calculation of $K(t)$ and $P(E)$ through Eqs. (2) and (3). We begin by noting that when using the low frequency form for Z_ℓ in (9), both parts of $\text{Re}[Z_t(\omega)]$ have the same form, namely

$$\text{Re}[Z_t(\omega)] = \frac{R}{1 + \omega^2 \tau^2} \quad (16)$$

for appropriate R and τ . Calculations for $K(t)$ and $P(t)$ for this form have been given in detail elsewhere,^{30,31} but emphasize a different range for R and result in different forms for $P(E)$. Using

$$\frac{1}{\omega} \frac{R}{1 + \omega^2 \tau^2} = \frac{R}{\omega} - \frac{R\tau^2 \omega}{1 + \omega^2 \tau^2} \quad (17)$$

and $\coth(\hbar\omega/2k_B T) = 1 + 2/[\exp(\hbar\omega/k_B T) - 1]$ we find that

$$K(t) = R_Q^{-1} \left\{ \mathcal{F}_c \left[\frac{R}{\omega} \right] - \int \mathcal{F}_s \left[\frac{2R}{\exp(\hbar\omega/k_B T) - 1} \right] dt - i \text{sign}(t) \mathcal{F}_s \left[\frac{1}{\omega} \frac{R}{1 + \omega^2 \tau^2} \right] - \mathcal{F}_c \left[\frac{R\tau^2 \omega}{1 + \omega^2 \tau^2} \coth \left(\frac{\hbar\omega}{2k_B T} \right) \right] \right\} \quad (18)$$

where $\mathcal{F}_c[f(\omega)] = 2 \int_0^\infty f(\omega) \cos \omega t d\omega$ and $\mathcal{F}_s[f(\omega)] = 2 \int_0^\infty f(\omega) \sin \omega t d\omega$ are the Fourier cosine and sine transforms of $f(\omega)$ respectively, taken to be functions of $|t|$. We have ignored terms in $K(t)$ independent of t ; since for $P(E)$ to satisfy the normalization condition $\int_{-\infty}^\infty P(E) dE = 1$ we must have $K(0) = 0$,²⁴ we will later ensure normalization by adding an appropriate constant in any case.

Of the four terms in curly braces in Eq. (18) for $K(t)$, the first three can all be evaluated analytically.¹⁹ An analytic form for the entire kernel has also been found,³⁰ and analyzed for the overdamped case such that $1/\tau$ is large compared to the Josephson frequency $\omega_J = \pi\Delta/\hbar$. However, the range of R and τ in which we are interested was not investigated. Nevertheless, we have made some progress in certain limits. We note first that the fourth term in (18) depends on the temperature T only through the dimensionless combination $\mathcal{T} = \hbar/(2k_B T\tau)$, and write

$$\mathcal{F}_c \left[\frac{\tau^2 \omega}{1 + \omega^2 \tau^2} \coth \left(\frac{\hbar \omega}{2k_B T} \right) \right] = k_{\mathcal{T}}(t, \mathcal{T}) \quad (19)$$

For zero temperature ($\mathcal{T} = \infty$), we have

$$k_{\mathcal{T}}(t, \infty) = \sqrt{\pi} G_{13}^{21} \left(\frac{t^2}{4\tau^2} \middle| \begin{matrix} 0 \\ 0, 0, \frac{1}{2} \end{matrix} \right) \quad (20)$$

where G is a Meijer G function. In the long time limit, this result goes as $-(\tau/t)^2$.

More generally, for $T \neq 0$, we find that it is important to consider the relative importance of the terms in Eq. (18). If we evaluate the integrals which we can treat analytically, we have

$$K(t) = -\frac{2R}{R_Q} \left\{ \frac{\pi k_B T |t|}{\hbar} + \ln(1 - e^{-2\pi k_B T |t|/\hbar}) + \gamma - \ln 2 + i \frac{\pi}{2} \text{sign}(t) [1 - e^{-|t|/\tau}] + \frac{1}{2} k_{\mathcal{T}}(t, \mathcal{T}) \right\} \quad (21)$$

where $\gamma \approx 0.577216$ is Euler's constant. In order to compare the relative size of the terms, we evaluate $k_{\mathcal{T}}$ numerically. We find that for $\mathcal{T} \gg 1$, (either low temperature or small τ), $k_{\mathcal{T}}$ decays slowly with time. For long times then the term going as $e^{-|t|/\tau}$ is by far the smallest, and can be neglected. Of the remaining terms, in the long time limit the logarithmic term dominates over $k_{\mathcal{T}}$ and we write the kernel as

$$K_l(t) = -\frac{2R}{R_Q} \left\{ \frac{\pi k_B T |t|}{\hbar} + \ln(1 - e^{-2\pi k_B T |t|/\hbar}) + i \frac{\pi}{2} \text{sign}(t) - \ln(\pi/\mathcal{T}) \right\} \quad (22)$$

where the constant term $\ln(\pi/\mathcal{T})$ will allow $P(E)$ to be approximately normalized. This is essentially the result¹⁹ of Wilhelm, *et al.*, and is generally appropriate for dealing with the high-frequency part of Eq. (15) due to the relatively small values of Z_{2D} and C_{eff} . However, this

form may also be used for a sufficiently short and narrow section of transmission line.

In the opposite limit, for which $\mathcal{T} < 1$, we find that the approximate analytic result

$$k_{\mathcal{T}}(t, \mathcal{T}) \approx \pi e^{-|t|/\tau} \cot \mathcal{T} \quad (23)$$

holds for times $|t|/\tau > \mathcal{T}$. For typical temperature scales available in a dilution refrigerator ($T = 20\text{--}400$ mK), the logarithmic term is very small when (23) is applicable. We can therefore neglect it, and find¹⁸ that

$$K_s(t) = -\frac{2R}{R_Q} \left\{ \pi k_B T |t|/\hbar + \frac{\pi}{2} [\cot(\mathcal{T}) - i \text{sign}(t)] (e^{-|t|/\tau} - 1) \right\} \quad (24)$$

This result is typically most useful for dealing with finite RC lines, for which τ^{-1} is typically on the order of 10^7 s^{-1} .

Finally, for $1 \lesssim \mathcal{T} \lesssim 10$, both the logarithmic term and $k_{\mathcal{T}}$ are of the same magnitude for the relevant time scales. The analytic forms for $K(t)$ in (22) and (24) must then neglect some potentially important term.

2. Calculation of $P(E)$

Having obtained analytic forms for $K(t)$, a straightforward application of Eq. (3) allows one to calculate $P(E)$. Letting $g = R_Q/R$, we have from Eq. (22) for the large \mathcal{T} limit

$$P_l(E) = \frac{(\pi/\mathcal{T})^{2/g}}{2\pi^2 k_B T} \text{Re} \left[e^{-\pi/g} B \left(\frac{1}{g} - \frac{iE}{2\pi k_B T}, 1 - \frac{2}{g} \right) \right] \quad (25)$$

where $B(x, y)$ is the beta function, in agreement with Wilhelm, *et al.*¹⁹ For Z_{2D} we have from (15) that $R = \kappa_2 Z_{2D}$ and $\tau = \kappa_2 C_{\text{eff}} Z_{2D}$. While (25) is only valid for $g > 1$, in terms of Z_{2D} this condition becomes $Z_{2D} < R_Q/\kappa_2$, so that the result remains valid for quite large Z_{2D} when κ_2 is small.

In the small \mathcal{T} limit, we use (24) to obtain¹⁸

$$P_s(E) = \frac{\tau}{\pi \hbar} e^{\gamma_3(\mathcal{T}, g)} \text{Re} \left[e^{-i\pi/g} \gamma_2(\mathcal{T}, g)^{-\gamma_1(\mathcal{T}, g)} \times \{ \Gamma(\gamma_1(\mathcal{T}, g)) - \Gamma(\gamma_1(\mathcal{T}, g), \gamma_2(\mathcal{T}, g)) \} \right] \quad (26)$$

where $\Gamma(x, y)$ is the incomplete gamma function, and $\gamma_1 = \frac{\pi}{g} \mathcal{T} - i \frac{E\tau}{\hbar}$, $\gamma_2 = \frac{\pi}{g} (\cot \mathcal{T} - i)$ and $\gamma_3 = \frac{\pi}{g} \cot \mathcal{T}$. Typically, this will be applied to a finite RC line, for which $R = \kappa_1 r_\ell \ell$ and $\tau = r_\ell c_\ell \ell^2 / \sqrt{6}$. In some cases, for a short RC line, it may be more correct to use $P_l(E)$, and substitute the appropriate forms for R and τ in Eq. (25) instead.

We show $P_s(E)$ in Fig. 2(b) for the same transmission line parameters as used in Fig. 2(a). For comparison, we also show the $T = 0$ form for an infinite transmission line given by $P_{\text{inf}}(E) = \sqrt{eV_0/2\pi E^3} e^{-eV_0/2E}$ where

$eV_0 = (4r_\ell\kappa_1/R_Q)(e^2/2c_\ell)$. Even at $T = 10$ mK, $P_s(E)$ is significantly broader than $P_{\text{inf}}(E)$. While it is possible to obtain an analytic form for $P_{\text{inf}}(E)$ by expanding Eq. (2) in the high temperature limit, the resulting expression is of limited use for $E \neq 0$, since it involves only even powers of E and therefore cannot satisfy detailed balance.²⁴ As a result, such an expression cannot be used to calculate I - V characteristics, for instance, whereas $P_s(E)$ in (26) can.

Ultimately, we are interested in calculating $P_{\text{tot}}(E)$ for the total impedance $\text{Re}[Z_t(\omega)]$ seen by the tunneling electrons. If we were to calculate the total kernel $K(t)$ for the decomposition in (15), it would in general include all the terms in (21). We were unable to find an analytic form for $P_{\text{tot}}(E)$ under those circumstances. However, given the decomposition (15), it is possible to write $K(t) = K_{\text{lf}}(t) + K_{\text{hf}}(t)$ where $K_{\text{lf}}(t)$ and $K_{\text{hf}}(t)$ correspond to the low- and high-frequency parts of $\text{Re}[Z_t(\omega)]$, with corresponding $P_{\text{lf}}(E)$ and $P_{\text{hf}}(E)$. The total $P(E)$ is then given by the convolution $P(E) = P_{\text{lf}}(t) * P_{\text{tot}}(E) = \int_{-\infty}^{\infty} P_{\text{lf}}(E - E')P_{\text{hf}}(E')dE'$, which can be performed numerically.

C. Multisection Transmission Lines

In our particular case, the sample leads do not have a single width. Instead, they broaden in sections from $0.4 \mu\text{m}$ (section 1) to $375 \mu\text{m}$ (section 4) as detailed in Table II below. As a result, we must generalize (9) to allow for the possibility of multiple sections. In general, we use Eq. (7) for a loaded transmission line, beginning closest to the SET with section 1. For this section, Z_L is taken to be the impedance of the second section, which is in turn terminated by the following sections. This cascading process is taken to end at our macroscopic contact pads, which are so broad as to provide very little impedance, and we therefore take $Z_L = 0$ for the last section, so that its impedance is given by (8). We also ignore a short ($\ell = 1 \mu\text{m}$) section with $w = 100$ nm since it contributes only 50Ω to $Z_\ell(0)$, and its associated $P(E)$ is very sharply peaked around $E = 0$.

If we were to use the exact form for Z_ℓ given by the above cascading procedure, it would be too complex to be of use. Fortunately, a simple approximation gives fairly accurate results. We take

$$\text{Re}[Z_\ell(\omega)] = \sum_i \frac{r_{\ell_i}\ell_i}{1 + (\omega r_{\ell_i}c_{\ell_i}\ell_i^2/\sqrt{6})^2} \quad (27)$$

where r_{ℓ_i} and c_{ℓ_i} are the resistance and capacitance per unit length of section i , and ℓ_i is its length. We use the width w_i and length ℓ_i of each section along with the 2DEG sheet resistance $R_{sq} = 20 \Omega$ and depth $h = 50$ nm to calculate³² $r_{\ell_i} \approx R_{sq}/(w_i + 5.8h)$ and $c_{\ell_i} \approx \epsilon\epsilon_0(w_i/h + 1.393)$, where $\epsilon = 13$ is the dielectric constant of GaAs. To find an approximate form for $\text{Re}[Z_t(\omega)]$ we use the result (27) for Z_ℓ in the decomposition (15). For comparison, we plot both this approximate

TABLE II: Transmission line parameters for the various sections of the sample leads, with w and ℓ in μm , r_ℓ in $\text{M}\Omega/\text{m}$, c_ℓ in nF/m , $r_\ell\ell$ in Ω , and \mathcal{T} calculated for $T = 100$ mK.

section	w	ℓ	r_ℓ	c_ℓ	$r_\ell\ell$	\mathcal{T}
1	0.4	9	29	1.08	260	37
2	1	57	15.5	2.46	884	0.76
3	10	253	1.9	23	491	3.2×10^{-2}
4	20	375	1.0	46	375	1.5×10^{-2}

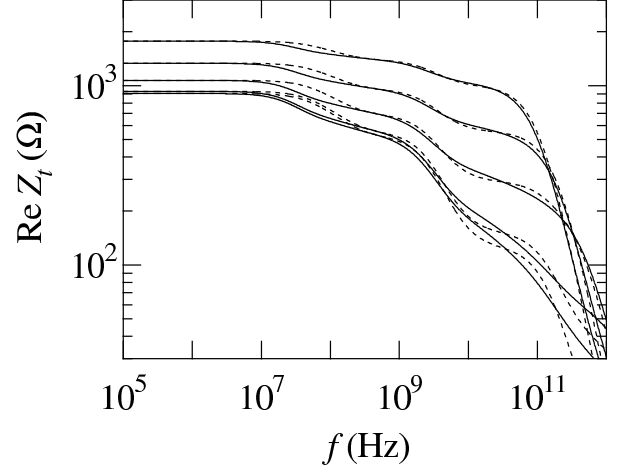


FIG. 3: $\text{Re}[Z_t(\omega)]$ for four cascaded RC lines and a ground plane, using the parameters given in Table II, for (top to bottom) $Z_{2D} = 6445, 3227, 1291, 258$ and 100Ω . Solid lines: exact calculation of $\text{Re}[Z_t(\omega)]$. Dashed lines: approximate version of $\text{Re}[Z_t(\omega)]$ as described in the text.

result as well as the exact one obtained from the full form for $\text{Re}[Z_t(\omega)]$ in (4)–(6) and repeated applications of (7) versus frequency in Fig. 3 for different values of Z_{2D} . The agreement is very good, especially considering the number of approximations required to develop a tractable approximate form for $\text{Re}[Z_t(\omega)]$. The approximate version tracks the exact result very well except between the various corner frequencies of the transmission line sections, where its slope is generally too small. Agreement is better overall for larger values of Z_{2D} , but even for the smallest values is still acceptable.

We can calculate $P_\ell^{(j)}(E)$ for tunneling through junction j for the four section transmission line by choosing either $P_l(E)$ or $P_s(E)$ for a given section based on its value of \mathcal{T} in Table II, and numerically convolving the four functions through

$$P_\ell^{(j)}(E) = P_{1l}^{(j)}(E) * P_{2s}^{(j)}(E) * P_{3s}^{(j)}(E) * P_{4s}^{(j)}(E). \quad (28)$$

While somewhat time consuming, this procedure needs to be performed only once for a given temperature since the 2DEG beneath the transmission lines is not affected by the Au gates, and so the transmission line parameters do not change with V_g .

Finally, we then calculate the total $P_{\text{tot}}^{(j)}(E)$ for tun-

neling through junction j by convolving $P_\ell^{(j)}(E)$ with $P_{2D}^{(j)}(E)$ calculated from $P_\ell(E)$ for the appropriate value of Z_{2D} . This procedure typically must be performed many times, but can be done relatively quickly. Results for $P_{\text{tot}}^{(1)}(E)$ for tunneling through junction 1 of S2 are shown in Fig. 4 for a series of different values of Z_{2D} . For $Z_{2D} = 0$, we take $P_{\text{tot}}^{(1)}(E) = P_\ell(E)$, which is already relatively broad, with a width several microvolts. In contrast, for small Z_{2D} , $P_{2D}^{(1)}(E)$ is very sharply peaked around $E = 0$ and approximates a delta function, as can be seen in the insets (a) and (b) in Fig. 4. As a result, $P_{\text{tot}}^{(1)}(E)$ is not strongly affected by $P_{2D}^{(1)}(E)$ until $Z_{2D} \gtrsim 200 \Omega$. Finally, for sufficiently large Z_{2D} , $P_{2D}^{(1)}(E)$ begins to dominate and $P_{\text{tot}}^{(1)}(E)$ becomes very broad, indicating the high probability of inelastic transitions. Overall, the trend is for the transmission line to dominate energy exchange for small Z_{2D} , while the 2DEG dominates energy exchange for large Z_{2D} .

D. Calculation of I - V Curves

To calculate the I - V characteristics for the S-SET, we use a master equation approach²⁵ in which we assume that only two charge states, N and $N + 1$ where N is the number of Cooper pairs, are important. This should be a valid approach for temperatures and biases small compared to the charging energy E_c of the S-SET. We begin by calculating the free energy change for changing the island charge from N to $N + 1$ (or vice versa) due to tunneling through junction j . We find

$$\begin{aligned} \delta f_{N \rightarrow N+1}^{(j)} &= -\delta f_{N+1 \rightarrow N}^{(j)} \\ &= 4E_c(2N - n_g + 1) - (-1)^j 2\alpha_j eV \end{aligned} \quad (29)$$

where $n_g = V_g C_g / e$ is the gate charge and $\alpha_j = \frac{1}{2} + (-1)^j (C_1 - C_2) / 2C_\Sigma$ is the fraction of the bias voltage V appearing across junction j . We then use Eq. 1 to find the tunneling rates in terms of the sample parameters.

The master equation can be solved exactly when only two charge states are considered.²⁵ Doing so, and using the detailed balance relation $P(-E) = e^{-E/k_B T} P(E)$, we find

$$I(V) = \frac{\pi^2 \Delta^2}{32eR_K} \frac{\sinh\left(\frac{eV}{k_B T}\right)}{\frac{\tilde{r}_2^2}{P_2} \cosh\left(\frac{\delta f^{(1)}}{2k_B T}\right) + \frac{\tilde{r}_1^2}{P_1} \cosh\left(\frac{\delta f^{(2)}}{2k_B T}\right)} \quad (30)$$

where $\delta f^{(j)}$ is the change in free energy for tunneling in the electrostatically favorable direction ($N + 1 \rightarrow N$ for junction 1 and $N \rightarrow N + 1$ junction 2), $\tilde{r}_j = R_j / R_K$, $\tilde{P}_j = (P_j^+ P_j^-)^{1/2}$, $P_j^\pm = P_{\text{tot}}^{(j)}(\mp \delta f^{(j)})$, and $R_K = h/e^2$ is the resistance quantum.

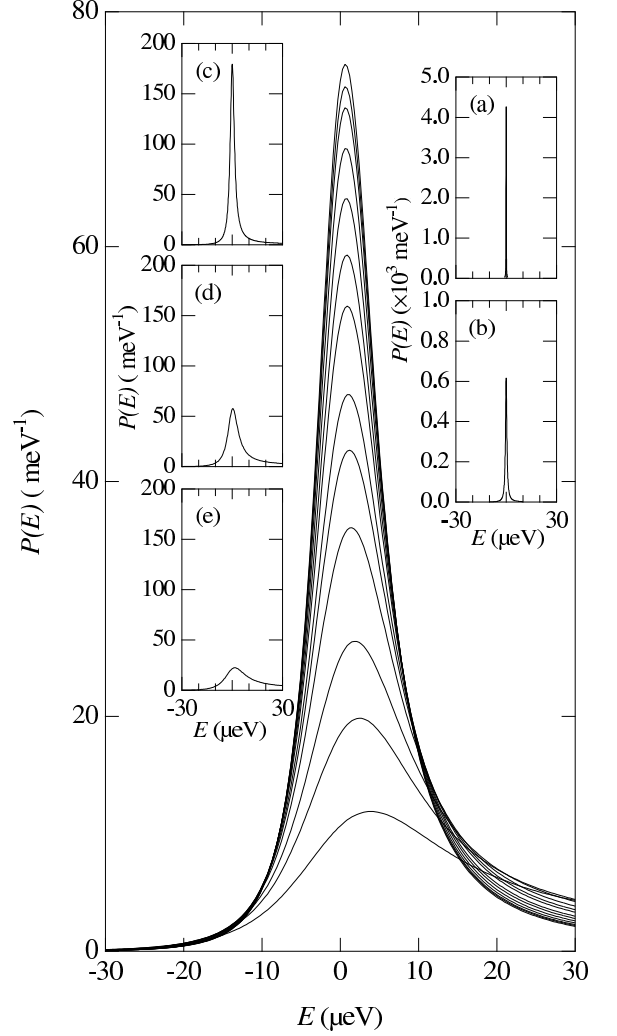


FIG. 4: Calculated $P_{\text{tot}}^{(1)}(E)$ for S2, based on the transmission line parameters from Table II for a series of values of Z_{2D} . Top to bottom: $Z_{2D} = 0, 65, 129, 258, 430, 645, 860, 1291, 1613, 2151, 3227, 4302$ and 6445Ω . Insets: $P_{2D}^{(1)}(E)$ for Z_{2D} equal to (a) 65 (b) 430 (c) 1291 (d) 3227 and (e) 6445 Ω . Note the scale change for $Z_{2D} = 65$ and 430Ω .

III. EXPERIMENTAL RESULTS

A. Measurements

We have performed electrical measurements on the two samples described in Table I in a dilution refrigerator at mixing chamber temperatures ranging from $T = 20$ to 400 mK. Measurements were performed in a four-probe voltage biased configuration, with the bias applied symmetrically with respect to ground, in a shielded room using battery powered amplifiers. High frequency noise was excluded with π -filters at room temperature and microwave filters at the mixing chamber.

Because the S-SET and 2DEG are electrically isolated from each other at dc, we were able to measure their

conductances G_{SET} and $G_{2\text{D}}$ separately. In both cases the conductance was measured by applying an ac bias voltage at 11 Hz and measuring the resulting current using standard lock-in techniques. The bias voltage used was 3 and 5 μV respectively for the S-SET and 2DEG. We also performed measurements of dc I - V characteristics of the S-SET. For the 2DEG, the current contacts were positioned on opposite sides of the two QPCs, so that $G_{2\text{D}}$ measured the series combination of their conductances. Since the S-SET sees the QPCs in parallel, we take $Z_{2\text{D}} = 1/(4G_{2\text{D}})$ for the pool geometry. For the stripe geometry we cannot measure the stripe resistance R_{str} or capacitance C_{str} directly, although we can estimate them from the sample design. We expect that in this geometry $Z_{2\text{D}} \approx R_{\text{QPC}}/2$ at low frequencies and $Z_{2\text{D}} \approx R_{\text{str}}/2 \approx 100 \Omega$ at high frequencies, as discussed above. While the I - V measurements of the S-SET were usually performed at a fixed gate voltage V_g , the conductance measurements were typically performed versus V_g for a variety of temperatures. In the pool geometry all six Au gates were tied together and V_g swept from 0 to -1 V, while in the stripe configuration only the four outermost gates were swept.

Results of these measurements are shown for S2 in Fig. 5 for mixing chamber temperatures ranging from 50 to 200 mK. As V_g is made more negative, the S-SET conductance oscillates due to the effects of the Coulomb blockade; the oscillations are clearly visible in Fig. 5(a)–(e). We show results for the pool geometry for various temperatures in Fig. 5(a)–(d), and results for the stripe geometry in Fig. 5(e). In both geometries, the envelope of the oscillations is relatively flat until $V_g \approx -0.3$ V, at which point the amplitude of oscillations begins to increase. For the pool geometry, the envelope continues to rise until $V_g \lesssim -0.4$ V, at which point it begins to fall again. For the lower temperatures ($T < 100$ mK), the drop with more negative V_g is quite steep, whereas for the higher temperatures ($100 \text{ mK} < T < 200 \text{ mK}$) the drop is more gradual. For less negative V_g , the envelope generally rises as T decreases, and tends to saturate below $T \approx 100$ mK. For more negative V_g (beyond the maximum in the envelope at $V_g = -0.41$ V) the envelope rises as T decreases until $T \approx 100$ mK, below which it decreases.

Since $G_{2\text{D}}$ decreases as V_g becomes more negative, the above behavior indicates that G_{SET} varies non-monotonically as $G_{2\text{D}}$ decreases, first rising and then falling. A decrease in G_{SET} as $G_{2\text{D}}$ decreases is expected. Physically, a larger $G_{2\text{D}}$ tends to damp phase fluctuations, promoting superconducting behavior and therefore a higher G_{SET} . Alternatively, we can say that for low energies, the probability $P(E)$ of exchanging energy with the environment increases as $G_{2\text{D}}$ increases, as can be seen in Fig. 4. A higher $G_{2\text{D}}$ therefore implies a higher probability of elastic (or nearly elastic) transitions, and a higher G_{SET} at low bias. In contrast, the decrease in G_{SET} for $V_g \gtrsim -0.4$ V does not fit in with this general picture of energy exchange with the environment. While

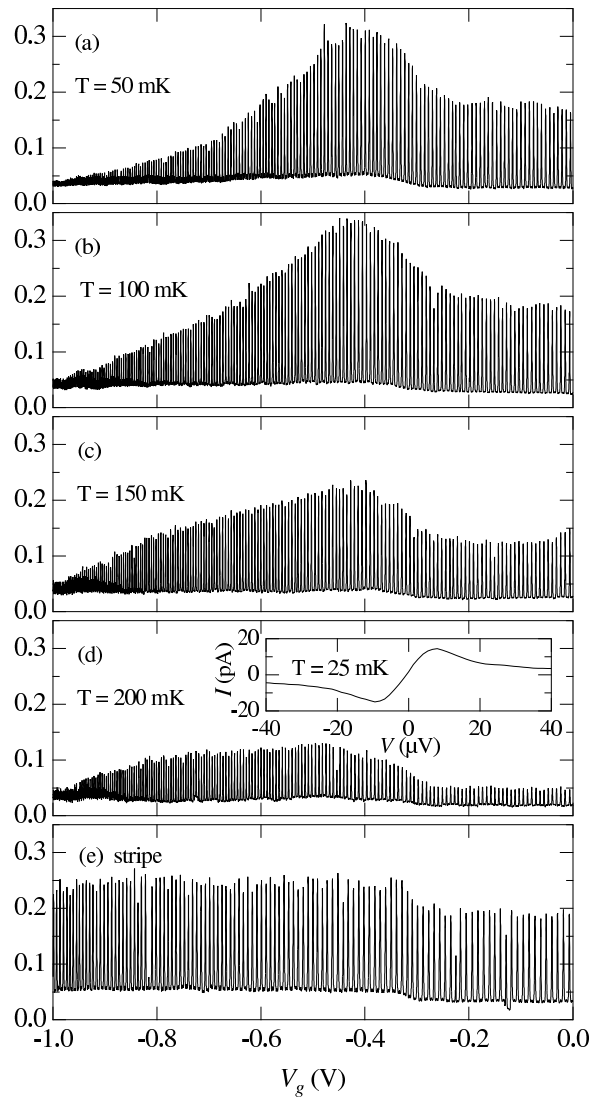


FIG. 5: G_{SET} vs. V_g for S2 in the pool geometry for $T =$ (a) 50, (b) 100, (c) 150, and (d) 200 mK. In (e) we show G_{SET} vs. V_g in the stripe geometry for $T = 25$ mK. The inset to (d) shows an I - V characteristic for S2 at $T = 25$ mK with the 2DEG left unconfined ($V_g = 0$ V).

nonmonotonic behavior with $G_{2\text{D}}$ can be expected,¹⁹ it is generally associated with a crossover from the non-linear to linear portions of the I - V characteristic. We find that this is true in our simulations as well.

In contrast, for our experiments G_{SET} was always measured in the linear part of the I - V characteristic. We show in the inset to Fig. 5(d) the I - V characteristic for S2 at $T = 20$ mK for $V_g = 0$ V, *i. e.*, when the 2DEG is unconfined. The I - V characteristic is clearly linear to $\pm 8 \mu\text{V}$, so that our 3 μV rms bias should be firmly in the linear regime. The non-monotonic behavior we observe cannot then be associated with changes in $P(E)$, and must arise from other physics.

We can find a clue as to the source of this behavior by examining G_{SET} vs. V_g for the stripe geometry as shown

in Fig. 5(e). In this geometry the envelope also begins to rise at $V_g \approx -0.3$ V. However, the rise is weaker, with the envelope increasing by only roughly half what is observed in the pool geometry. Furthermore, there is no decline in G_{SET} as V_g is made more negative. This last observation is in agreement with our model for $Z_{2\text{D}}$ in this geometry, which predicts that $Z_{2\text{D}}$ approaches $R_{\text{str}}/2$ at the higher frequencies which dominate our measurement of G_{SET} . As a result, in this case $P_{\text{tot}}(E)$ never broadens for more negative V_g as it does in the pool geometry, so that no decrease in G_{SET} is observed. Once again, the environmental theory cannot explain the reduction in G_{SET} for less negative V_g .

One possible explanation for this decrease is that there are changes in the offset charge of the S-SET island that occur on a time scale short in comparison to the time constant of the lock-in, but long in comparison to the time scales associated with environmental fluctuations. It is well known that charge fluctuations in the substrate give rise to $1/f$ noise in SET-based electrometers.^{33,34} Such charge noise typically has a magnitude of $(S_Q)^{1/2} \sim 10^{-4} - 10^{-3} e/\sqrt{\text{Hz}}$ at 10 Hz and a cut-off frequency (above which the intrinsic SET noise dominates) of about 100–1000 Hz. Let us assume that in our case the $1/f$ noise is somewhat larger than is typical, say $(S_Q)^{1/2} \sim 4 \times 10^{-3} e/\sqrt{\text{Hz}}$ at 10 Hz, due to the presence of the 2DEG. If we write $S_Q = 1.6 \times 10^{-4} e^2/f \equiv S_0/f$, then the expected mean square charge variance³⁵ between frequencies f_1 and f_2 is given by $\langle \sigma_{ch}^2 \rangle = S_0 \ln(f_2/f_1)$. Taking $f_1 = 0.1$ Hz and $f_2 = 1000$ Hz we find $\langle \sigma_{ch}^2 \rangle^{1/2} \sim 4 \times 10^{-2} e$, so that a typical variance of a few hundredths of an electronic charge is not unreasonable.

In a voltage biased configuration such as ours, these fluctuations would have the effect of averaging the measured current over an ensemble of charge states centered around the gate charge n_g . Similar effects have been seen in measurements of other S-SET systems.³⁶ Since the S-SET current is sharply peaked around the charge degeneracy points, we expect that any such charge averaging would tend to reduce the measured peak current, and therefore the conductance G_{SET} . It is therefore possible that the reduction in G_{SET} for less negative V_g arises due to increased charge averaging as the electrons in the 2DEG become less confined. We examine this possibility in more detail in the following section.

B. Comparison with Theory

To compare our measurements with theory, we must plot the measured G_{SET} versus $G_{2\text{D}}$. Having measured $G_{2\text{D}}$ versus V_g , we can fit a smooth function to the measured $G_{2\text{D}}$ and use it to convert V_g to an approximate $G_{2\text{D}}$. In Fig. 6(b) below we show both the measured $G_{2\text{D}}$ and the fitted function versus V_g in units of conductance quanta $G_0 = e^2/h$. While the two are nearly indistinguishable in the figure, this procedure is only useful for a limited voltage range. For $V_g \gtrsim -0.31$ V ($G_{2\text{D}} \gtrsim 200 G_0$)

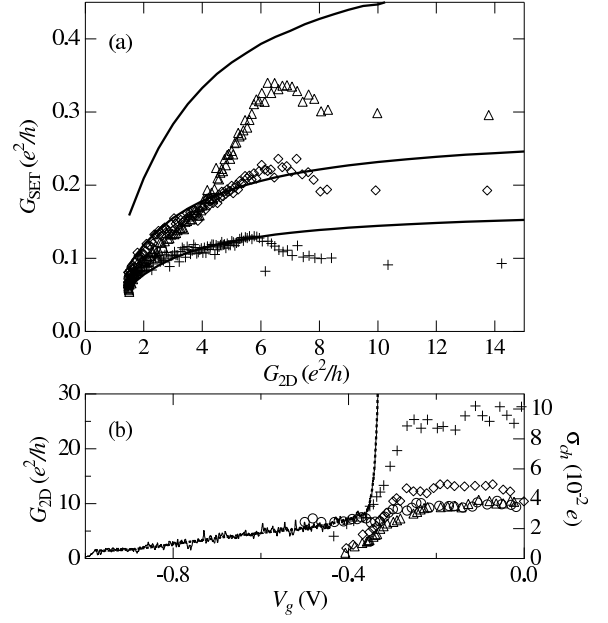


FIG. 6: (a) Peak values of G_{SET} versus $G_{2\text{D}}$ for $T = 100$ mK (Δ), 150 mK (\diamond), and 200 mK ($+$). Calculated values G_{SET}^c scaled to equal G_{SET} at its maximum value at $G_{2\text{D}}^{\text{max}}$ at 200 mK are shown as the heavy solid lines. (b) On the left axis we plot measured $G_{2\text{D}}$ versus V_g (solid line), and the smooth function fitted to $G_{2\text{D}}$ vs. V_g (heavy dashed line). On the right axis we plot values of σ_{ch} in the pool geometry for $T = 100$ mK (Δ), 150 mK (\diamond), and 200 mK ($+$). We also show σ_{ch} for the stripe geometry (\circ).

the measured values of $G_{2\text{D}}$ become unreliable.

Having converted V_g to $G_{2\text{D}}$ we must now plot the envelope of G_{SET} versus $G_{2\text{D}}$; we do so by recording the positions of the peaks in G_{SET} versus V_g and using our fitting function to convert to $G_{2\text{D}}$. The results of this process are shown for $T = 100, 150$ and 200 mK in Fig. 6(a). As can be seen in Fig. 5, our data show no sign of $2e$ periodicity,^{37,38,39,40} even at the lowest temperatures. A similar lack of $2e$ periodicity was observed by the Berkeley group as well.¹⁶ At the present time, it is unknown whether this is an intrinsic feature of S-SET/2DEG systems or is due to the inherent difficulties of excluding high-frequency noise from all possible sources, including the substrate.⁴¹ In any case, we presume that since our data are strictly e -periodic that probabilities of finding the S-SET island with either an even or odd number of electrons are approximately equal. This will have little overall effect on our analysis, since at any given value of n_g only one charge state contributes significantly to the current, the other being between charge degeneracy points and therefore in a low-current regime. Overall, we would then expect an additional reduction of a factor of roughly two in the measured current above and beyond that due to any other reason.

In order to compare our results with theory, we calculate $P_{\text{tot}}(E)$ according to the procedure described in Section II C above. We then use (30) above to obtain a cal-

culated conductance G_{SET}^c . In general, the conductance calculated directly from (30) overestimates the measured conductance G_{SET} by a significant factor (on the order of 40–50). Such discrepancies are not uncommon in small tunnel junction systems,^{16,36,37} but nevertheless complicate comparison with theory. The best we can achieve is to compare the relative change in G_{SET} and G_{SET}^c , but to do so requires that we pick some point of reference at which we will scale G_{SET}^c to make it equal to G_{SET} .

G_{SET} reaches its maximum value at some value of $G_{2\text{D}}$ which for all the temperatures considered here is approximately $6.5G_0$; we call this value $G_{2\text{D}}^{\text{max}}$, which may vary slightly with temperature. For $G_{2\text{D}} > G_{2\text{D}}^{\text{max}}$, G_{SET} decreases, behavior which cannot be accounted for through changes in the environment, making this region unsuitable for choosing a reference point. For $G_{2\text{D}} < G_{2\text{D}}^{\text{max}}$, we assume for simplicity that there is no charge averaging, and choose the point at which G_{SET} reaches its maximum at $T = 200$ mK as our reference point.

We plot G_{SET}^c versus $G_{2\text{D}}$, choosing our reference point as discussed above, in Fig. 6(a) as the heavy solid lines. All curves are scaled by the same factor (≈ 44) so that we can get some sense of the agreement in terms of temperature dependence as well as dependence on $Z_{2\text{D}}$. Generally speaking, the agreement at $T = 150$ and 200 mK is quite good for $G_{2\text{D}} < G_{2\text{D}}^{\text{max}}$; both calculated curves for G_{SET}^c track the experimental values of G_{SET} nearly exactly. We note that to obtain this level of agreement, we have used only one variable parameter, namely the scaling factor. All other parameters used in the theory are derived from experimentally measured quantities. Given the number of approximations involved, the level of agreement for these two temperatures is quite remarkable.

For temperatures higher than $T = 200$ mK, the S-SET conductance begins to rise again. However, we expect the environmental theory discussed here to be applicable only for temperatures satisfying the Coulomb blockade condition³⁰ $k_B T \ll E_c R_Q / (2\pi^2 \text{Re}[Z_t(0)])$, which for S2 corresponds to $T \approx 240$ mK for typical values of $\text{Re}[Z_t(0)]$. Failure of the theory between $T = 200$ and 250 mK is in good agreement with this condition.

At $T = 100$ mK and below, the theory also disagrees with the experimental results. Specifically, the measured G_{SET} does not rise as rapidly with decreasing T as predicted by theory. Furthermore, the dependence of G_{SET} on $G_{2\text{D}}$ changes from sublinear to superlinear, so that the S-SET conductance depends more strongly on the environmental impedance than theory predicts. This trend is accentuated at lower temperatures, as can be seen in Fig. 5(a) for $T = 50$ mK. In this case G_{SET} is an even stronger function of $G_{2\text{D}}$, and G_{SET} is generally speaking slightly smaller than at $T = 100$ mK (not larger as would be expected from the theory). One possible explanation for a saturation of G_{SET} would be that the electron temperature stops decreasing for some temperature below 100 mK. While it is likely that our electron temperature saturates (data at 20 mK differs only very slightly from the 50 mK data), such effects would not

explain the change in dependence on $G_{2\text{D}}$, or a decrease in G_{SET} from 100 to 50 mK.

There is also a lower temperature bound for applicability of the environmental theory, set by the condition $P_{\text{max}}^{(i)} E_{J_i} \ll 1$ where $P_{\text{max}}^{(i)}$ is the maximum value of $P_{\text{tot}}^{(i)}(E)$. This condition must be satisfied for the perturbative result for the tunneling rate in Eq. (1) to be satisfied. In our case, we find that for tunneling through junction 1 (for which both E_J and P_{max} are larger), $P_{\text{max}}^{(1)} \approx 52, 41$ and 34 meV⁻¹, all at $G_{2\text{D}} = 6.5G_0$ and at $T = 100, 150$ and 200 mK, respectively. In that case we find that $P_{\text{max}}^{(1)} E_{J_1} = 1.4, 1.1$, and 0.92 for the same temperatures. In none of the cases is the condition for agreement with Eq. (1) clearly satisfied, so that the agreement at 150 and 200 mK is perhaps better than might be expected. Still, if it were a failure of the perturbative expansion which is leading to the disagreement at 100 mK, we would expect the theory to agree for sufficiently low $G_{2\text{D}}$ that P_{max} drops to its largest value at 150 mK. In our case, this occurs at $G_{2\text{D}} \approx 4.0G_0$ so that based on this argument we would expect theory and experiment to agree at 100 mK over much of the range shown, and only deviate for $4.0G_0 < G_{2\text{D}} < 6.5G_0$. Clearly, this expectation does not hold for our data.

We now turn our attention to the range $G_{2\text{D}} > G_{2\text{D}}^{\text{max}}$, for which G_{SET} decreases, in contradiction to the environmental theory. As discussed above, we consider the possibility that some form of charge averaging, which increases as $G_{2\text{D}}$ increases and the electrons in the 2DEG become more mobile, causes G_{SET} to decline. To test the plausibility of this hypothesis, we calculate the average conductance $\langle G_{\text{SET}}^c \rangle$ given by

$$\langle G_{\text{SET}}^c \rangle = \int_{-\infty}^{\infty} w(n') G_{\text{SET}}^c(V, n') dn' \quad (31)$$

where $G_{\text{SET}}^c(V, n)$ is the calculated SET conductance (including the scaling factor) calculated at bias V and gate charge n and $w(n) = \frac{1}{\sqrt{2\pi}\sigma_{ch}} \exp\left[-\frac{(n-n_g)^2}{2\sigma_{ch}^2}\right]$ is assumed to be the probability of finding the SET in charge state n when the gate charge is n_g . We vary σ_{ch} to cause the $\langle G_{\text{SET}}^c \rangle$ to exactly match the measured conductance at a given V_g and plot the results in Fig. 6(b) for $T = 100, 150$, and 250 mK in the pool geometry, and a mixing chamber temperature of 20 mK for the stripe geometry (estimated electron temperature roughly 50–70 mK). By construction, $\sigma_{ch} = 0$ for $G_{2\text{D}} < G_{2\text{D}}^{\text{max}}$ in the pool geometry. For the stripe geometry, σ_{ch} saturates at about $2 \times 10^{-2}e$ for large negative V_g , since in this geometry G_{SET} never reaches as large a value as it does in the pool geometry. This result is physically reasonable, since the electrons in the stripe are never as confined as they are in the pool. As V_g becomes less negative, σ_{ch} rises until it saturates (in all cases) at $V_g \approx -0.27$ V, the voltage at which the 2DEG begins to deplete. The saturation value for σ_{ch} is generally reasonable, being about $4 \times 10^{-2}e$ for the stripe and for the the pool at 100 mK, and $5 \times 10^{-2}e$

and $9 \times 10^{-2}e$ at 150 and 200 mK. While the cause of the increase in σ_{ch} at 200 mK is unclear, there does not appear to be significant further rise in σ_{ch} for higher temperatures.

To provide further support for this idea, we examine I - V characteristics for S1 as shown in Fig. 7(a), which show the evolution of the I - V characteristics when the 2DEG is increasingly confined. As the confinement is increased, the current initially rises ($V_g = -0.3$ V) at all voltages, while the peak current remains at a fixed voltage. For $Z_{2D} = 1613 \Omega$, the current has increased again, but the peak current has begun to move to higher bias. For $Z_{2D} = 2151 \Omega$, the peak current has decreased and moved again to yet higher bias, while the current at higher voltages has generally begun to rise. Finally for $Z_{2D} = 6453 \Omega$ the I - V characteristic has become quite broad and the peak has moved outward yet again.

We can understand this evolution by examining the effects of variations in Z_{2D} and σ_{ch} on the I - V characteristics separately, as shown in Fig. 7(b) and (c) respectively. When Z_{2D} alone is increased, the peak current drops and the voltage at which the peak occurs increases; at the same time, current at higher biases increases. This reflects broadening of $P_{tot}(E)$ as Z_{2D} is increased, and a higher probability of inelastic processes. In contrast, when σ_{ch} alone is increased, the current decreases at all bias voltages, and the voltage at which the maximum current appears is more or less fixed.

In order to obtain good agreement with experiment, we must include both variations in σ_{ch} and Z_{2D} , as shown in Fig. 7(d). Here, for $V_g = 0$ and -0.3 V, we take $Z_{2D} = 0$ and vary σ_{ch} , while for $Z_{2D} = 1613, 2151$, and 6453Ω we take $\sigma_{ch} = 0$. Overall the theory agrees with the experimental results quite well (apart from an overall scaling factor), reproducing the initial rise in current with no shift in peak current position, followed by a reduction in current and an outward shift in peak position. The agreement is poor only for $Z_{2D} = 6453 \Omega$, for which the experimental current is too large in relative terms. Even here, however, the shape of the I - V curve is reproduced nicely. Additional data (not shown) indicates that the S-SET current does usually drop sharply for large Z_{2D} , so that the amplitude of this particular I - V curve is probably anomalously high.

C. Discussion

Overall, the agreement between our experimental results and calculations seems quite good, particularly for $T = 150$ and 200 mK. The good agreement of G_{SET}^c and G_{SET} for those temperatures, combined with the accurate predictions of our model for the evolution of the I - V characteristics gives us confidence that our model, despite its complexity, accurately describes our experimental system. In particular, it is clear that both the lead impedance and any impedance which is coupled directly to the S-SET island must be included to give ac-

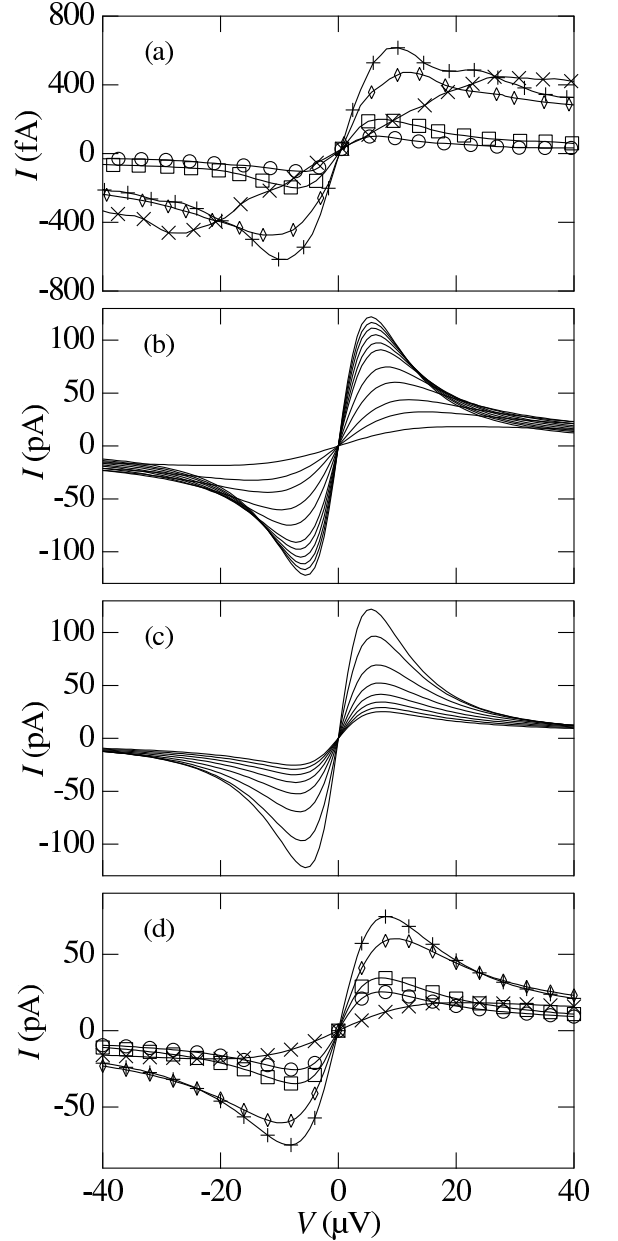


FIG. 7: (a) I - V characteristics for S1 at an estimated electron temperature of 100 mK for an unconfined 2DEG (\circ), $V_g = -0.3$ V (\square), and $Z_{2D} = 1613$ (+), 2151 (\diamond) and 6453 Ω (\times). (b) Calculated I - V characteristics (top to bottom at peak) for $Z_{2D} = 0, 129, 258, 430, 645, 860, 1613, 2151, 3227, 4302$ and 6453 Ω . Here $\sigma_{ch} = 0$ for all curves. (c) Calculated I - V characteristics for (top to bottom) $\sigma_{ch} = 0, 1, 2, 3, 4, 5, 6$ and $7 \times 10^{-2}e$. Here $Z_{2D} = 0$ for all curves. (d) Calculated I - V characteristics for an unconfined 2DEG (\circ), $V_g = -0.3$ V (\square), and $Z_{2D} = 1613$ (+), 2151 (\diamond) and 6453 Ω (\times). To fit the data at $V_g = 0$ and -0.3 V, we use $\sigma_{ch} = 0.07$ and $0.05e$, respectively. For the remaining curves we take $\sigma_{ch} = 0$.

curate results. In our particular case, charge averaging appears to play an important role when the confinement of the 2DEG is reduced, either for less negative V_g or when the stripe geometry is used. Overall, this improved understanding indicates that S-SET/2DEG systems can be used to test the accuracy of the standard environmental theory in a way which was not previously possible.

Generally speaking, the model of the environment presented in (15) should be applicable to any system consisting of an S-SET and its leads fabricated above a 2DEG, including that of the Berkeley group. The model also gives a simple explanation for the lack of agreement between the experimental results of the Berkeley group and the scaling theory of Wilhelm, *et al.* Since neither the leads nor the 2DEG can be ignored, $P_{\text{tot}}(E)$ must be a convolution of $P_\ell(E)$ and $P_{2D}(E)$. In that case, our own calculations indicate that the power law behavior described in Wilhelm, *et al.*, does not survive the convolution. The resulting dependence of G_{SET} on G_{2D} does however resemble power law behavior over a limited range of G_{2D} , with an exponent which can vary with temperature. Whether charge averaging effects are important in the Berkeley system is unclear to us at this time.

The most significant puzzle associated with our own work is the sudden disagreement between theory and experiment between $T = 150$ and 100 mK. While it is clear that the perturbative expression for the tunneling rates in Eq. 1 has a low temperature bound for applicability, it is unclear why theory and experiment disagree at 100 mK for *all* $G_{2D} < 6.5G_0$. This disagreement, as well as the continued reduction in current for temperatures below 100 mK is suggestive either of a limitation in the environmental theory, or that some other physics is beginning to dominate at the lowest temperatures. Note that while Z_{2D} becomes relatively large, the impedance seen by the junctions never becomes much larger than about 1000Ω at any frequency since both κ_1

and κ_2 are relatively small, so that we are still in the low impedance limit $\text{Re}[Z_t(\omega)] < R_Q$. Difficulties with the environmental theory in this impedance range could be of great importance to potential quantum computation applications. Finally, we do not believe that Coulomb blockade physics in the 2DEG is likely to be of importance, since the QPC conductances are still quite high even for the smallest values of G_{2D} ; Coulomb blockade oscillations do not begin to appear in the 2DEG until both QPCs have a conductance below G_0 .

It is straightforward to propose experiments which could address these issues. The simplest would be to perform more measurements like those in Fig. 5 for samples with smaller E_J . (Such measurements were unfortunately not performed for S1). One could also simplify the analysis significantly by constructing samples in which the 2DEG is selectively removed beneath the leads. In that case, the leads would no longer act as transmission lines, and would present a small impedance to the tunneling electrons, so that in all probability only G_{2D} would be of importance. We can also imagine reducing the coupling capacitance C_{2D} so as to reduce the effective environmental impedance and keep the S-SET current relatively large even for large Z_{2D} . This could be particularly useful if the 2DEG is further confined so as to form a quantum dot, in which case the S-SET could be used to probe the dot impedance and energy level structure.

Acknowledgments

This research was supported at Rice by the NSF under Grant No. DMR-9974365 and by the Robert A. Welch foundation. One of us (A. J. R.) acknowledges support from the Alfred P. Sloan Foundation. We thank K. D. Maranowski and A. C. Gossard for providing the 2DEG material.

-
- ¹ Yu. Makhlin, G. Schön, and A. Shnirman, *Nature* **398**, 305 (1999).
 - ² Y. Nakamura, Yu. A. Pashkin, and J. S. Tsai, *Nature* **398**, 786 (1999).
 - ³ J. E. Mooij, T. P. Orlando, L. Levitov, L. Tian, C. H. van der Wal, and S. Lloyd, *Science* **285**, 1036 (1999).
 - ⁴ D. Vion, A. Aassime, A. Cottet, P. Joyez, H. Pothier, C. Urbina, D. Esteve, and M. H. Devoret, *Science* **296**, 886 (2002).
 - ⁵ A. Shnirman, G. Schön, and Z. Hermon, *Phys. Rev. Lett.* **79**, 2371 (1997).
 - ⁶ Yu. Makhlin, G. Schön, and A. Shnirman, *Rev. Mod. Phys.* **73**, 357 (2001).
 - ⁷ T. Fujisawa, T. H. Oosterkamp, W. G. van der Wiel, B. W. Broer, R. Aguado, S. Tarucha, and L. P. Kouwenhoven, *Science* **282**, 932 (1998).
 - ⁸ R. Aguado and L. P. Kouwenhoven, *Phys. Rev. Lett.* **84**, 1986 (2000).
 - ⁹ S. L. Sothdhi, S. M. Girvin, J. P. Carini, and D. Shahar, *Rev. Mod. Phys.* **69**, 315 (1997).
 - ¹⁰ N. Mason and A. Kapitulnik, *Phys. Rev. Lett.* **82**, 5341 (1999).
 - ¹¹ A. Kapitulnik, N. Mason, S. A. Kivelson, and S. Chakravarty, *Phys. Rev. B* **63**, 125322 (2001).
 - ¹² A. J. Rimberg, T. R. Ho, Ç. Kurdak, J. Clarke, K. L. Campman, and A. C. Gossard, *Phys. Rev. Lett.* **78**, 2632 (1997).
 - ¹³ V. Bouchiat, D. Vion, P. Joyez, D. Esteve, and M. H. Devoret, *Phys. Scripta* **T76**, 165 (1998).
 - ¹⁴ H. Grabert and M. H. Devoret, eds., *Single Charge Tunneling* (Plenum, New York, 1992).
 - ¹⁵ E. Turlot, D. Esteve, C. Urbina, J. M. Martinis, M. H. Devoret, S. Linkwitz, and H. Grabert, *Phys. Rev. Lett.* **62**, 1788 (1989).
 - ¹⁶ J. B. Kycia, J. Chen, R. Therrien, Ç. Kurdak, K. L. Campman, A. C. Gossard, and J. Clarke, *Phys. Rev. Lett.* **87**,

- 017002 (2001).
- ¹⁷ W. Lu, K. D. Maranowski, and A. J. Rimberg, Phys. Rev. B **65**, 060501 (2002).
 - ¹⁸ W. Lu, K. D. Maranowski, and A. J. Rimberg, cond-mat/0204287.
 - ¹⁹ F. K. Wilhelm, G. Schön, and G. T. Zimányi, Phys. Rev. Lett. **87**, 136802 (2001).
 - ²⁰ W. Lu, A. J. Rimberg, K. D. Maranowski, and A. C. Gosard, Appl. Phys. Lett. **77**, 2746 (2000).
 - ²¹ G.-L. Ingold, P. Wyrowski, and H. Grabert, Z. Phys. B **85**, 443 (1991).
 - ²² A. A. Odintsov, G. Falci, and G. Schön, Phys. Rev. B **44**, 13 089 (1991).
 - ²³ V. Ambegaokar and A. Baratoff, Phys. Rev. Lett. **10**, 486 (1963).
 - ²⁴ G.-L. Ingold and Yu. V. Nazarov, in¹⁴, pp. 21–107.
 - ²⁵ G. Schön, in *Quantum Transport and Dissipation* (Wiley-VCH, Weinheim, Germany, 1998), pp. 149–212.
 - ²⁶ D. V. Averin, Yu. V. Nazarov, and A. A. Odintsov, Physica B **165&166**, 945 (1990).
 - ²⁷ H. Grabert, G.-L. Ingold, M. H. Devoret, D. Estève, H. Pothier, and C. Urbina, Z. Phys. B **84**, 143 (1991).
 - ²⁸ D. M. Pozar, *Microwave Engineering, 2nd Ed.* (John Wiley & Sons, New York, 1998).
 - ²⁹ L. S. Kuzmin, Yu. V. Nazarov, D. B. Haviland, P. Delsing, and T. Claeson, Phys. Rev. Lett. **67**, 1161 (1991).
 - ³⁰ H. Grabert, G.-L. Ingold, and B. Paul, Europhys. Lett. **44**, 360 (1998).
 - ³¹ H. Grabert and G.-L. Ingold, Supperlattices and Microstruct. **25**, 915 (1999).
 - ³² R. E. Collin, *Foundations for Microwave Engineering* (McGraw-Hill, New York, 1992).
 - ³³ E. H. Visscher, S. M. Verbrugh, J. Lindeman, P. Hadley, and J. E. Mooij, Appl. Phys. Lett. **66**, 305 (1995).
 - ³⁴ V. A. Krupenin, D. E. Presnov, M. N. Savvateev, H. Scherer, A. B. Zorin, and J. Niemeyer, J. Appl. Phys. **84**, 3212 (1998).
 - ³⁵ Sh. Kogan, *Electronic Noise and Fluctuations in Solids* (Cambridge University Press, Cambridge, United Kingdom, 1996).
 - ³⁶ T. M. Eiles and J. M. Martinis, Phys. Rev. B **50**, 627 (1994).
 - ³⁷ M. T. Tuominen, J. M. Hergenrother, T. S. Tighe, and M. Tinkham, Phys. Rev. Lett. **69**, 1997 (1992).
 - ³⁸ T. M. Eiles, J. M. Martinis, and M. H. Devoret, Phys. Rev. Lett. **70**, 1862 (1993).
 - ³⁹ A. Amar, D. Song, C. J. Lobb, and F. C. Wellstood, Phys. Rev. Lett. **72**, 3234 (1994).
 - ⁴⁰ P. Joyez, P. Lafarge, A. Filipe, D. Esteve, and M. H. Devoret, Phys. Rev. Lett. **72**, 2458 (1994).
 - ⁴¹ M. Covington, M. W. Keller, R. L. Kautz, and J. M. Martinis, Phys. Rev. Lett. **84**, 5192 (2000).